Statistical and neural network assessment of the climatology of fog and mist at Pula airport in Croatia

Marko Zoldoš*[1,2], Tomislav Džoić*[3], Jadran Jurković[2], Frano Matić[4], Sandra Jambrošić[2], Ivan Ljuština[2], Maja Telišman Prtenjak[5]

[1]Risk Management Division, Erste & Steiermärkische Bank d.d., Rijeka 51000, Croatia (ORCID: 0009-0005-1117-5716)
[2]Aviation Meteorology department, Croatia Control Ltd., Velika Gorica 10410, Croatia
[3]Laboratory of Physical Oceanography, Institute of Oceanography and Fisheries, Split 21000, Croatia (ORCID: 0000-0001-9585-8779)
[4]University Department of Marine Studies, University of Split, Split 21000, Croatia (ORCID: 0000-0003-0392-4172)
[5]Department of Geophysics, Faculty of Science, University of Zagreb, Zagreb 10000, Croatia (ORCID: 0000-0002-4941-8278)

*Leading author: Marko Zoldoš, correspondence to: Tomislav Džoić (dzoic@izor.hr)

Abstract. A study was conducted on the climatological characteristics of fog and mist at Pula Airport in the northeastern Adriatic, using statistical and machine learning approaches. The study utilized meteorological data from Pula Airport, along with satellite sea surface temperature (SST) data from two coastal areas west and east of the airport, to gain insights into the influence of sea temperature on fog formation. To identify weather patterns associated with the occurrence of fog and mist, wind and mean sea-level pressure (MSLP) data from the ERA5 reanalysis were analyzed using Growing Neural Gas (GNG), a machine learning method. A notable finding was a declining trend in the frequency of fog and mist at the airport, which can be linked to the results of the GNG analysis of the ERA5 data. This analysis showed a decrease in synoptic patterns favorable for fog and mist. Fog occurs mainly between October and March and is primarily associated with weak westerly and northwesterly winds. Additionally, fog is more likely to occur when the sea surface temperature is higher than the air temperature. Mist has similar characteristics to fog, although it is more likely to occur with easterly winds.

1 Introduction

According to the World Meteorological Organization (WMO), fog is the suspension of very small water droplets or ice crystals in the atmosphere, reducing visibility on the Earth's surface to less than 1 km (WMO, 1966). The formation of these water droplets and ice crystals is influenced by factors such as cooling, increased humidity, and the mixing of air masses with different temperatures (Gultepe et al., 2007). Mist, a related phenomenon, occurs when horizontal visibility at the surface is between 1 and 10 km, with aviation meteorology specifically defining mist as conditions where visibility is between 1 and 5 km. Fog is a unique atmospheric phenomenon confined to the atmospheric boundary layer (ABL), the lowest part of the atmosphere, and its characteristics are influenced by the Earth's surface. The formation and dissipation of fog are impacted by synoptic and mesoscale conditions, as well as surface features such as moisture sources (e.g., oceans, lakes, rivers), vegetation, orography, urban areas, and sea currents.

This study examines fog occurrence over an extended period at Pula Airport, located in the coastal region of Croatia in the northeastern Adriatic (Figure 1). The Adriatic Sea is a large semi-enclosed sea separating the Apennine Peninsula from the Balkans. It is the northernmost arm of the Mediterranean Sea, extending from the Strait of Otranto (where it connects to the Ionian Sea and the rest of the Mediterranean) to the northwest, toward the Po Valley and the Istria Peninsula. This region frequently experiences marine fog due to synoptic-scale effects that can trigger subsidence within the boundary layer, which causes stratus clouds to descend to the surface. Similar marine fog events have been studied in the northwestern Pacific and Atlantic Oceans (e.g., Koračin et al., 2001; Koračin and Dorman, 2017). In the Adriatic, fog typically occurs between September and May, often disrupting sea transport and port operations (Popović et al., 2014). Fog also significantly affects air traffic at airports, where it can cause significant flight delays due to poor visibility and low cloud ceilings. These delays result in substantial financial losses for airlines, underscoring the need for accurate fog forecasting. For example, dense fog at New Delhi Airport in India caused losses of approximately 3.9 million U.S. dollars between 2011 and 2016 (Kulkarni et al., 2019). Improved fog forecasting could mitigate such losses, as illustrated by Allan (2001), who estimated that better forecasts for low-visibility events at three New York City airports could save up to $240,000 per event.

These factors highlight the critical role of fog research in advancing forecasting capabilities. Despite its importance, the study of fog remains an area of atmospheric science where our understanding is limited, both over land (Gultepe et al., 2007) and ocean (Koračin and Dorman, 2017). Fog formation involves a complex interaction of processes ranging from synoptic to microscale levels. The typical size of fog condensation nuclei is around 0.1 μm (10^{-5} cm), while the synoptic-scale processes that contribute to fog development occur on a scale of 10^8 cm or more, making the ratio of interacting length scales about 10^{13}. Fully understanding fog formation involves various elements, including large-scale synoptics (Belo-Pereira and Santos, 2016), characteristics of the surface and radiation exchange (Duynkerke, 1991), microphysics (Gultepe and Milbrandt, 2007; Wang et al., 2019), climatology (Stolaki et al., 2009; Veljović et al., 2015), relationships with turbulence intensity (Ju et al., 2020), presence of aerosol (Oztaner and Yilmaz, 2013), and more. The complicated interplay of meteorological parameters that determine whether fog forms or not poses a substantial challenge for accurate fog forecasting (Bergot and Koračin, 2021). In addition to local factors

75 influencing fog and mist formation, the impact of global warming and climate change cannot be overlooked. These

76 global phenomena have been linked to a reduction in the number of days with fog and mist (Kawai et al., 2016; Klemm

77 and Lin, 2016). Considering that fog occurrence in the eastern Adriatic has been studied infrequently, with the most

78 recent research conducted over 50 years ago (Stipaničić, 1972), there is a need for updated insights.

79

80 This study analyzes the climatological characteristics of fog at Pula Airport, Croatia, with a focus on understanding

81 the general patterns of fog initiation and dissipation. The primary objective is to provide detailed statistical analyses

82 to help understand the local and dynamic processes leading to fog development. A secondary objective is to assess the

83 influence of sea surface temperature (SST) in the vicinity of the study area on the frequency and intensity of advective

84 fog. SST has been shown to significantly impact the accuracy of numerical weather prediction (NWP) models (Huang

85 et al., 2022). To achieve these goals, the Growing Neural Gas Network (GNG), an unsupervised machine learning

86 algorithm within artificial neural networks (Martinetz and Schulten, 1991), was applied. This method classifies

87 synoptic conditions that prevail before and during the occurrence of fog at Pula into distinct weather patterns, and

88 identifies those that favor fog development. The results of this research could aid local forecasters in improving fog

89 prediction by accounting for specific terrain and coastline features, as well as synoptic and local influences

90 (particularly SST), thereby closing a gap in scientific knowledge about fog characteristics in this part of the

91 Mediterranean.

92 **2 Location, data and methods**

93 **2.1 Location**

94 Pula Airport, located approximately 6 km ENE of the coastal city of Pula in western Croatia (Figure 1b), serves as the

95 region's international airport. Its geographical coordinates are 44°53'37" N and 13°55'20" E, with an elevation of 84

96 meters above mean sea level (AMSL). In 2023, the airport served 413,439 passengers, ranking as the fifth busiest

97 airport in Croatia by passenger traffic (source: https://podaci.dzs.hr/2023/en/58556). The airport is situated at the

98 southern tip of the Istrian Peninsula—the largest peninsula in the Adriatic Sea—positioned between the Gulf of Trieste

99 to the northwest and the Kvarner Gulf to the east. The climate of Istria is influenced by Alpine and Dinaric Alps

100 mountain ranges and the Mediterranean Sea. Winters in Istria are typically mild and wet, while summers are hot and

101 humid. The interior of Istria experiences a more continental climate, while the coastal area is significantly influenced

102 by the Adriatic Sea. Recent research has analyzed bioclimatic parameters, highlighting these climatic boundaries

103 across the peninsula (e.g., Omazić et al., 2020).

104

105 Two weather patterns are primarily associated with fog in Pula. The first involves a westerly to northwesterly flow

106 that advects moist air under anticyclonic conditions. In these cases, advection can occur over a broad geographical

107 area. Fog is often advected from the Po Valley in northern Italy, where it is a frequent phenomenon during the fall-

108 winter season (Mariani, 2009), across the northern Adriatic to the Istrian coast. Under such conditions, fog can persist

109 for days across the affected region (Bendix, 1994). For example, Linate Airport in Milan, Italy, historically

110 experienced the highest number of annual closures due to fog among European airports (Mariani, 2009). While
111 advective fog is less common in the northwestern Adriatic, it still frequently occurs on the western coast of Istria
112 (Tešić and Brozinčević, 1974), which is climatologically the foggiest area of the eastern Adriatic (Stipaničić, 1972).
113 The second weather pattern associated with fog in Pula involves an easterly to southeasterly flow during a weakening
114 anticyclone, often advecting moist air from the southeast. These patterns are linked to the broader atmospheric
115 circulation over the Adriatic Sea, which is shaped by four dominant wind regimes. The northeasterly bora and the
116 southeasterly sirocco winds, both common in the colder months, are influenced by regional synoptic systems. In
117 contrast, during warmer months, sea/land breezes and, to a lesser extent, the Etesian wind, become more prominent.
118 The wind regime strongly influences changes in wind direction at Pula Airport (e.g., Pandžić and Likso, 2005; Prtenjak
119 and Grisogono, 2007; Prtenjak et al., 2010; Belušić et al., 2018).

120

121 The terrain surrounding the airport is predominantly flat, covered with grassland and small forested areas. There are
122 no significant hills or mountains nearby that would notably influence the local weather or climate. The central part of
123 the airport, along with its southern surroundings, lies within a very shallow basin, which is prone to nighttime
124 inversions during calm wind conditions and clear skies (as reported by local forecasters). The proximity of the sea
125 exerts a substantial influence on the airport's weather. Pula Bay is located 6 km to the west-southwest, while the open
126 waters of the northern Adriatic Sea are just 10 km away. To the east, the open sea is 7 km away, with the small Bay
127 of Kavran situated just 5 km from Pula Airport. These geographical factors contribute to the significant marine
128 influence on the weather at Pula Airport, even though the airport itself is not directly on the coast.

129

130

131
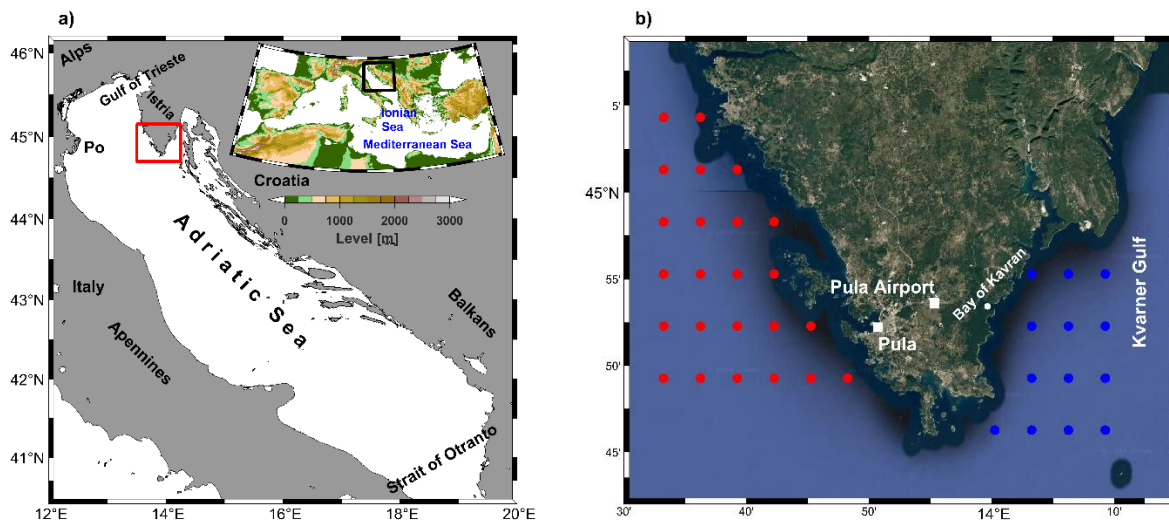
Figure 1. a) Map of the bathymetry of the Adriatic Sea, with the black square marking the Adriatic Sea area. The red rectangle on the map marks the immediate surroundings of Pula Airport (b) (© Google Maps 2024). The important localities are marked with white squares, while blue and red dots mark the eastern and western grid points from which the satellite SST values were extracted. The wider area of the Mediterranean Sea corresponds to the area of the ERA5 reanalysis.

2.2 Data and methods

The dataset used for this study includes half-hourly METAR reports and three-hourly SYNOP reports from the meteorological station at Pula Airport. METAR (METeorological Aerodrome Report) is a coded report describing weather conditions at the airport in a manner standardized for aviation. SYNOP (Surface Synoptic Observations) is a coded report describing weather conditions at a meteorological station. An airport meteorological station sends both SYNOP and METAR reports. The meteorological variables considered are wind speed and direction, temperature at 2 meters above ground, dew point temperature, relative humidity, surface pressure, cloud cover, and horizontal visibility. These variables are reported by both station observers and automatic instruments. The dataset spans a 20-year period from January 1, 2001, to December 31, 2020, with all measurements recorded at the airport's meteorological station. Runway 27, the primary operational runway, is equipped for Category I operations. This allows for takeoff and landing under low visibility conditions with a Runway Visual Range (RVR) of up to 550 meters or a ceiling height of 200 feet (approximately 60 meters). This capability underscores the operational challenges posed by fog: visibility below 550 meters prohibits aircraft landings and takeoffs.

In addition to the airport data, daily sea surface temperature (SST) measurements from the Pula Bay oceanographic station were included. These SST values, recorded at 07:00, 14:00, and 21:00 local time from January 1, 2001, to December 31, 2020, were supplemented with reprocessed satellite SST data from the Copernicus Marine Data Store (https://data.marine.copernicus.eu/). This gap-free dataset, which has been optimally interpolated with a grid resolution of 0.05° (Merchant et al., 2019), provides a comprehensive view of sea surface temperatures. Two coastal areas were selected for analysis: one to the west of the airport, encompassing the open Adriatic Sea, and the other to the east, covering the Kvarner Gulf (Figure 1). These regions were chosen to calculate the average spatial SST for a given day and evaluate their influence on fog formation. The selected areas are representative of the nearshore waters where the prevailing winds most frequently originate.

To identify the synoptic wind and pressure fields associated with fog occurrence at Pula Airport and across the Mediterranean region, 10-meter wind and mean sea-level pressure (MSLP) data were sourced from the fifth generation of ECMWF's ERA5 reanalysis. This reanalysis provides a comprehensive record of global climate and weather from the last 4 to 7 decades. ERA5 integrates observational data with atmospheric models to deliver detailed and accurate assessments of past weather. It has a horizontal resolution of 0.25° for latitude and longitude, a temporal resolution of one hour, and a vertical resolution based on 37 pressure levels (Hersbach et al., 2020a; 2020b). The study area spans from 6°W to 42°E and 30°N to 48°N (Figure 1a, inset map), encompassing the region where key synoptic processes influencing the Adriatic Sea predominantly occur. The analysis covers a 40-year period from 1979 to 2019, providing a comprehensive temporal dataset for assessing atmospheric conditions. At the same time, this area optimizes the calculation time.

172 To manage the large datasets of 10-meter wind and MSLP and classify them into spatio-temporal patterns that shed

173 light on atmospheric conditions favoring fog formation at Pula Airport, the Growing Neural Gas Network (GNG)

174 method was employed. GNG is an unsupervised artificial neural network that clusters high-dimensional input data by

175 reducing its dimensions and grouping it into best matching units (BMUs) (Fritzke, 1995). Unlike traditional neural

176 networks with fixed structures, GNG dynamically expands by adding new neurons in response to input patterns. This

177 ability to grow and adapt allows GNG to effectively cluster data and detect patterns and anomalies. The GNG

178 algorithm has been successfully used to detect anomalies in Adriatic Sea data, combining various biological and

179 oceanographic inputs (Šantić et al., 2021; Džoić et al., 2022).

180

181 In this study, the methodology described in Matić et al. (2022) was applied to a high-dimensional, hourly, 40-year

182 dataset comprising wind components u and v, analyzed separately for each month of the year. Prior to implementing

183 the GNG algorithm, the wind data was arranged in such a way that two columns represented the spatial variations of

184 u and v, while rows corresponded to temporal instances. Wind data over land was excluded and assigned as NaN

185 values to reduce calculation time. This exclusion did not affect the results, as the study's primary focus was on the

186 synoptic-scale influences that generate specific wind patterns conducive to the formation of fog and mist. Over the

187 sea, the winds are very homogeneous and are often directly related to large-scale synoptic systems such as cyclones

188 or anticyclones. Over land, the influence of topography and vegetation introduces noise, making it more difficult to

189 distinguish synoptic influences from local influences. The proximity of the airfield to the sea and the flat, low-lying

190 terrain in the direction of prevailing winds (Figure 1b) justified this simplification of calculations. The GNG algorithm,

191 implemented using the NeuPy Python library and parameterized following Matić et al. (2022), was used to calculate

192 9 BMUs per month for each month of the year. These BMUs were then linked to corresponding mean sea level pressure

193 (MSLP) fields. The temporal sequence of BMUs was utilized to compute an average pressure field for each BMU,

194 offering a detailed representation of atmospheric patterns associated with fog formation.

195

196 Data processing and visualization were conducted using Python and MATLAB, with MATLAB employing the

197 M_map mapping package (Pawlowicz, 2020), available at www.eoas.ubc.ca/~rich/map.html.

198

199

200

201

202

3 Results and discussion

3.1 Climatological analysis
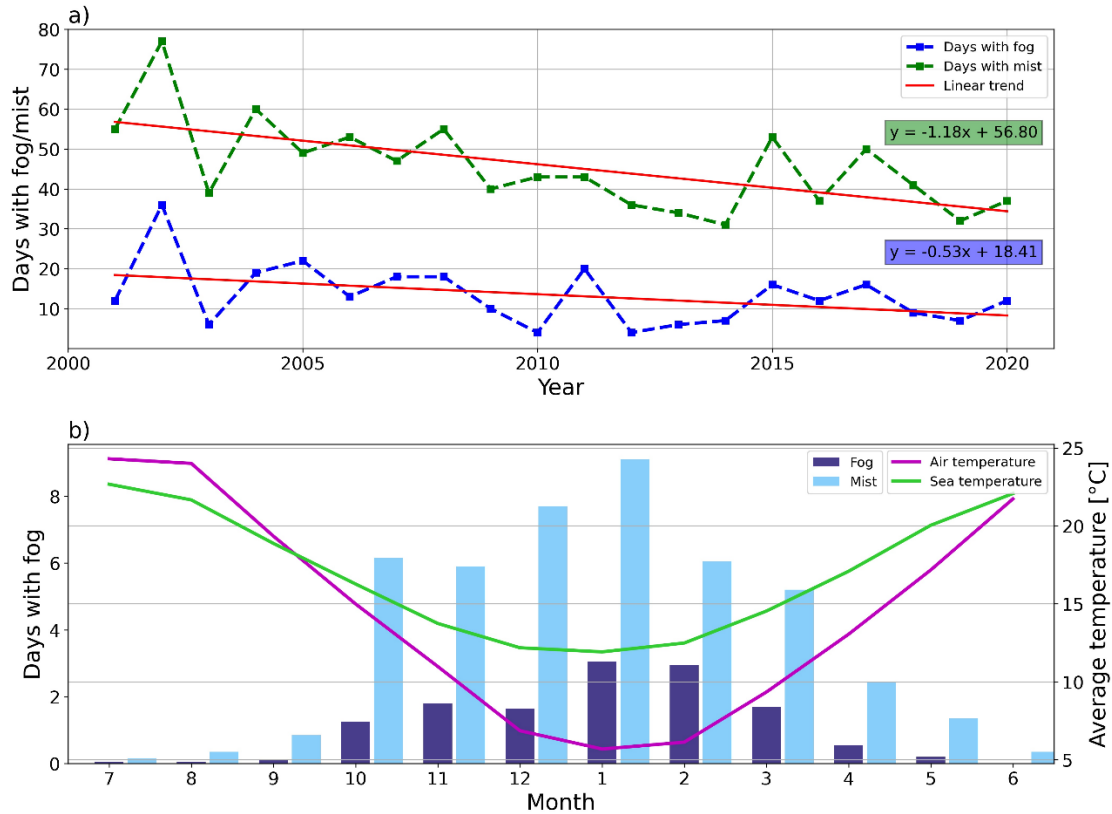
Figure 2. a) Annual number of days with fog (blue line) and mist (green line) at Pula Airport, 2001-2020. with associated linear trends and trend equations. b) Average monthly number of days with fog and mist at Pula Airport, the average sea temperature measured at the oceanographic station in Pula Bay and the average air temperature measured at the Pula Airport, 2001-2020. The graph is centered on the boreal winter.

To comprehensively analyze fog occurrence over Pula Airport, a climatological analysis was conducted at both large and small scales. Figure 2a illustrates the annual number of days with fog and mist from 2001 to 2020. A "fog day" is defined as any day with at least one METAR report indicating visibility below 1 km and the presence of fog at the airport. Similarly, a "mist day" is defined as any day with a METAR report indicating visibility between 1 km and 5 km, accompanied by mist observation, consistent with aeronautical meteorology definitions. This approach excludes cases where reduced visibility was caused by precipitation, such as rain or drizzle. On average, Pula Airport experiences 13.4 fog days and 45.6 mist days per year; however, this number is steadily decreasing, as indicated by the pronounced negative trend. The Mann-Kendall statistical significance test shows that this result is statistically significant at the 95% confidence level. A detailed evaluation of the linear trend indicates that the average number of fog days decreased by more than 10 days, from 18.4 in 2001 to 8.3 in 2020, with a slope coefficient of -0.53. Similarly, the average number of mist days declined by over 22 days, from 56.8 in 2001 to 34.4 in 2020, with a slope coefficient of -1.18. The larger absolute value of the slope coefficient for mist suggests that the average number of mist days is declining at a faster rate.

224   The observed statistically significant decreasing trend in the frequency of fog and mist at the airport is consistent with

225   similar findings in Europe, such as at Zagreb Airport (Zoldoš and Jurković, 2016) and Milano Airport (Mariani, 2009).

226   While the decrease in Zagreb and Milan is largely attributed to reduced air pollution, this conclusion is more

227   challenging to apply to Pula. As a smaller city with less industrial development, Pula's impact on neighboring

228   suburban and rural areas is not as pronounced. While a decrease in fog and mist frequency has been observed across

229   Europe, the effect is more prominent in continental Europe than in the Mediterranean region (Vautard et al., 2009).

230

231   Global warming and climate change are key drivers behind the long-term decline in fog frequency. Contributing

232   factors include rising temperatures in Pula and the surrounding Istria region (Bonacci, 2010; Šimunić et al., 2021),

233   increased sea surface temperatures (SST) throughout the Mediterranean (Pastor et al., 2018) and global trends in ocean

234   stratification (Li et al., 2020). Climate model reanalysis for the Adriatic Sea from 1987 to 2017 shows clearly positive

235   SST trends, especially in summer (Tojčić et al., 2023). Positive wind trends have been observed over the sea and along

236   the Adriatic Coast, between 0.1 and 0.2 m s-1 per decade (Tojčić et al., 2023), which could influence fog formation.

237   Furthermore, future projections suggest these changes will intensify, including lower wind speeds in coastal areas and

238   more extreme contrasts such as increased droughts and heavy precipitation events (Tojčić et al., 2024). Warmer SSTs

239   influence fog formation in two ways. Generally, they increase evaporation rates, enhancing fog advection when winds

240   are favorable. Additionally, in cases where fog forms with SST < SAT, they reduce the temperature gradient required

241   for fog development. In Pula, these favorable winds, which blow over the sea, play a significant role in fog and mist

242   formation.

243

244   A seasonal analysis (Figure 2b) reveals that over 90% of fog and mist events occur between October and March.

245   January accounts for the highest frequency of fog (23% of days) and mist (20% of days), followed by February (21%

246   and 13%, respectively), with December notable for mist (17%). In March, October, and November, fog and mist occur

247   on 12–13% of days. Fog is rare from April to May and almost absent from June to September; for example, no fog

248   was observed in June during the analyzed period. The annual distribution of fog at Pula Airport is also comparable to

249   the annual distribution of fog events at Zagreb Airport (Zoldoš and Jurković, 2016). A summary of the data shows

250   that during the climatological summer (June-July-August), fog occurrence can be expected approximately every six

251   years. Mist follows a similar seasonal pattern but is more frequent overall. In recent decades, January and February

252   have swapped positions as the months with the highest frequency of fog. While February used to be the foggiest month

253   at Pula Airport with an average of 3.5 foggy days (Stipaničić, 1972), climatological results have shown us that January

254   has become the foggiest month with 3.05 foggy days. The frequency of fog persistence, which is defined as fog

255   occurrence on two consecutive days, is shown in Figure 3. As expected based on previous findings about fog

256   characteristics, persistence can be expected only in the colder part of the year (October-April). From May to

257   September, there have been no recorded instances of fog occurring on two consecutive days. Stable anticyclonic

258   conditions during the cold season are most conducive to fog persistence.

259
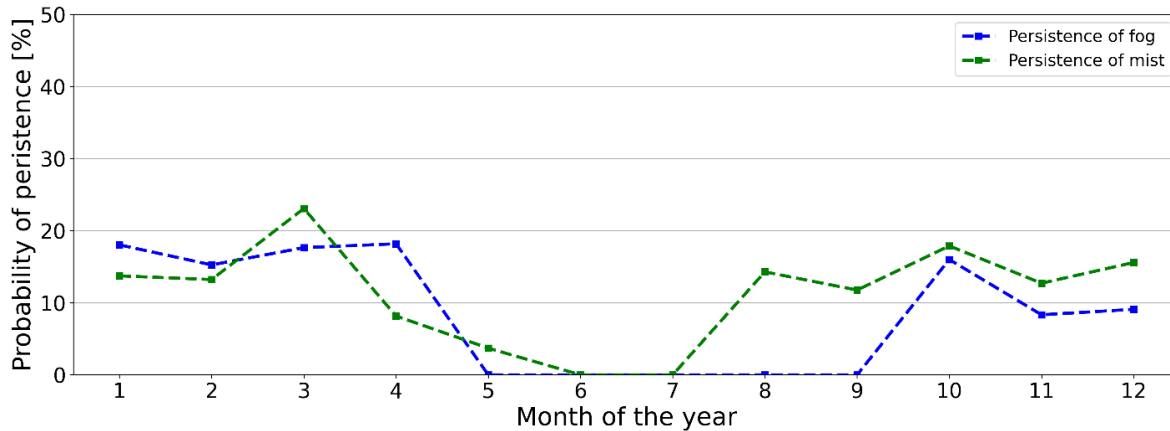
Figure 3. Yearly distribution of the climatological probability of persistence (fog occurrence on two consecutive days) of fog and mist at Pula Airport, 2001-2020. The probability of persistence is defined as the number of days with persistence relative to the total number of days with fog in a given month. Cases where a single fog event was present around midnight (and thus spanned two days) were not counted as persistence.

Wind is a critical factor influencing the formation and persistence of fog, as turbulence from wind shear significantly impacts the height of the stable boundary layer. To understand this relationship, the statistical characteristics of wind during fog episodes were analyzed. Figure 4 shows wind distributions (data from METAR reports) for all conditions and for fog/mist conditions in a wind rose plot. In general, the dominant wind at Pula Airport is the NE (*bora*), which can easily reach speeds greater than 10 m s^{-1}. Other frequently observed winds include westerlies, resulting from the interaction of Etesian winds with the sea breeze circulation (Pandžić and Likso, 2005; Klaić et al., 2009), as well as north-northeasterly and southeasterly winds. Winds from the northwest and southwest are relatively rare. The wind rose for fog conditions (Figure 4b) contrasts sharply with general conditions; W/NW winds are the most common (accounting for 47.7% of measurements). These winds blow from the direction of the open sea, whereas easterly winds blow from Kvarner Bay, characterized by deeper waters and numerous islands. In some cases, fog also forms under light easterly winds, typically below 3 m s^{-1}, although westerly fog events are often accompanied by wind speeds exceeding this threshold. Southerly winds are rarely associated with fog at Pula Airport.

Mist conditions show a different wind pattern (Figure 4c). Unlike fog, mist frequently occurs with easterly winds, which account for 28.8% of observations. This is consistent with the higher overall occurrence of mist compared to fog (Figure 2). Further analysis of the relationship between wind and visibility/cloud base in fog conditions (Figure 5a-d) highlights the rarity of fog in situations with northerly winds. The scatter plot of visibility and wind speed confirms the existence of an optimal range of wind speeds conducive to fog, with most fog events occurring at wind speeds between 0 and 2 m s^{-1}. The same is also observed for low clouds (lower than 200 m) — the majority of low cloud bases were observed at wind speeds of 1 m s^{-1} or less, some between 1 and 2 m s^{-1}, and very few cases at higher wind speeds. The absence of cloud bases above 300 m at wind speeds higher than 2 m s^{-1} is interesting. Higher wind speeds indicate stronger advection, and personal communication from forecasters suggests that in these cases cloud bases can be very low. This is particularly evident under westerly flows, where fog is more common and where wind speeds are higher. The data for mist conditions (Figure 5e-h) leads to similar conclusions for visibility—mist occurs

288 more frequently under westerly or easterly winds with slightly higher wind speeds than fog. Mist conditions with

289 cloud bases above 500 m do occur but are rare, and one noteworthy difference between mist and fog is the higher

290 number of mist events with a low cloud base during southeasterly and southwesterly winds.

291

292
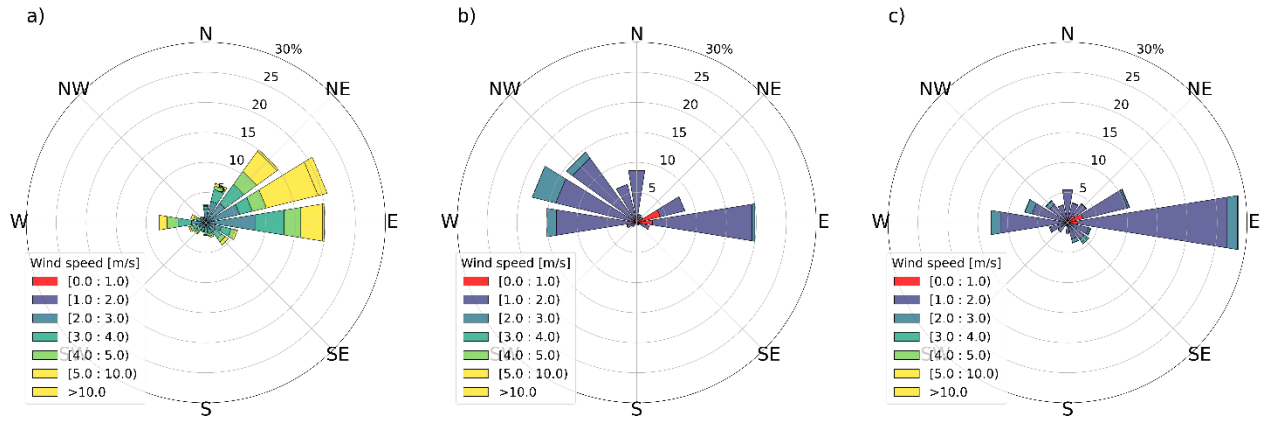
293 **Figure 4. Wind rose plots for Pula Airport, for dataset in the period 2001-2020: (a) the whole dataset, (b) fog conditions (c)**
294 **mist conditions. Data includes only reports where the variation in direction is less than 60° according to ICAO definition.**
295 **These account for 74 % of total data, 36 % of data in fog conditions and 39% of data in mist conditions.**

296
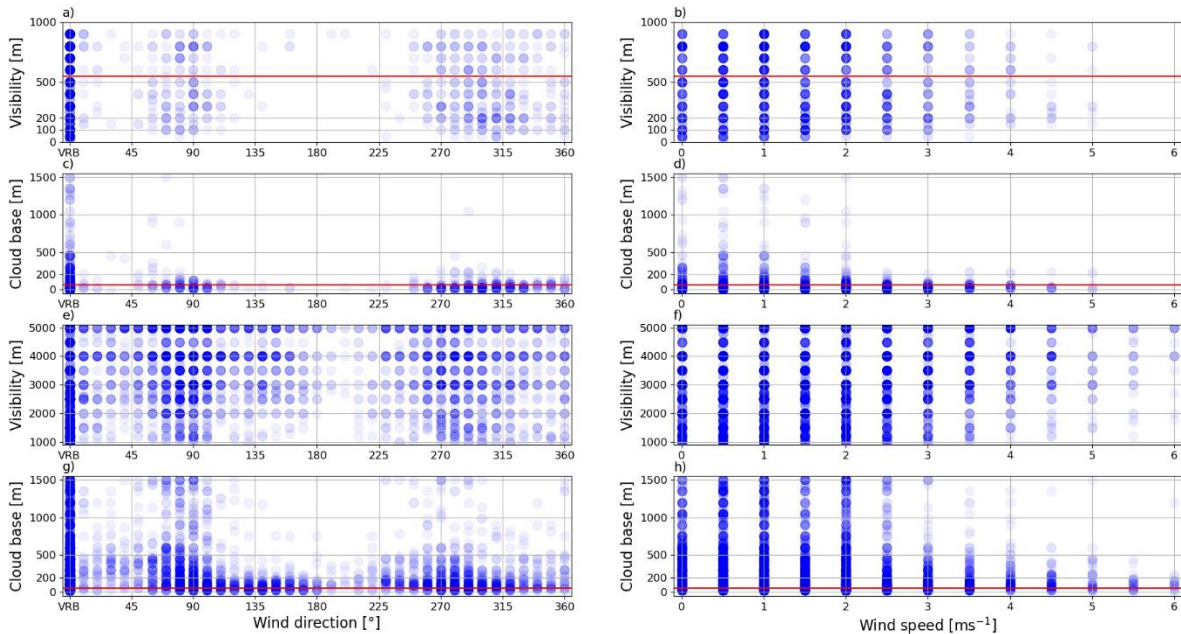
297 **Figure 5. Scatter plots of various meteorological parameters for fog conditions (a-d) and mist conditions (e-h) at Pula**
298 **Airport, 2001-2020. Circles are colored according to the frequency of data points (darker – more frequent). Red lines mark**
299 **the limits for Category I takeoff-landing procedures mentioned in Chapter 2. "VRB" denotes variable wind direction (180°**
300 **or more in a 2-minute interval) according to definition by ICAO (International Civil Aviation Organization).**

301
302
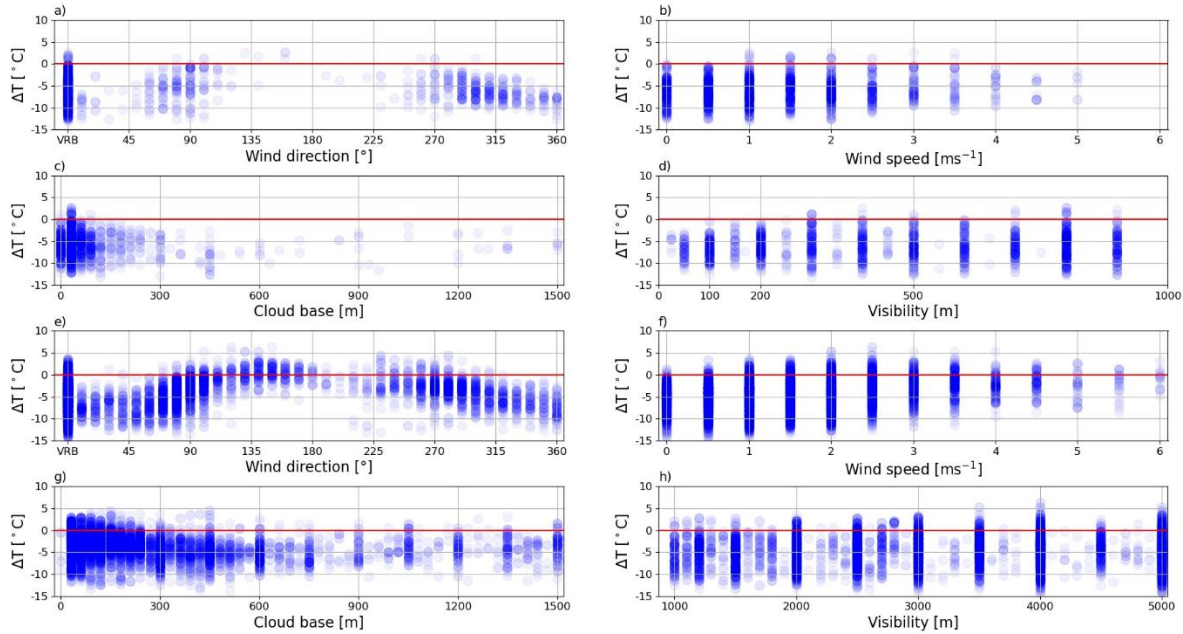
303
304 **Figure 6. Scatter plots of air-sea temperature difference between Pula Airport and Pula oceanographic station and various**
305 **meteorological parameters at fog initiation (a-d) and mist initiation (e-h), 2001-2020. Circles are colored according to the**
306 **frequency of data points (darker – more frequent). Red lines mark the 0 °C difference between air and sea temperature.**
307 **"VRB" denotes variable wind direction (180° or more in a 2-minute interval) according to definition by ICAO**
308 **(International Civil Aviation Organization).**

309

310 Fog occurrence can also be analyzed by examining conditions leading up to or at the time of its formation, as

311 demonstrated in previous studies (Tardif and Rasmussen, 2007; Veljović et al., 2015; Zoldoš and Jurković, 2016), or

312 by investigating the difference between air and sea surface temperature for marine fog (Li et al., 2022). In this study,

313 SAT data from METAR reports at Pula Airport were compared with SST measurements from the oceanographic

314 station in Pula Bay. Figures 6a-d depict scatterplots of SAT-SST differences and various parameters at fog initiation

315 (first METAR report with visibility <1000 m), while Figures 6e-h present similar data for mist initiation.

316

317 The majority of fog and mist events occur under negative SAT-SST differences, indicating that the sea surface is

318 warmer than the overlying air. Fog rarely forms during southerly winds, but mist is more common in these conditions,

319 particularly under southeasterly winds (Figure 6e). For southeasterly, southerly, and southwesterly winds with mist,

320 the SAT-SST difference tends to approach 0. Among fog events, 97.4% occured with negative SAT-SST differences,

321 with only 2.6% forming under conditions where SAT is equal to or warmer than SST. In mist cases, the proportion of

322 positive or zero SAT-SST differences is slightly higher (7.4%) but still strongly favors conditions with warm sea and

323 cooler air. At Pula Airport, fog is more common at wind speeds above 3 m s^{-1} than in continental areas such as Zagreb

324 Airport (Zoldoš and Jurković, 2016), but less common than in coastal regions such as California, where fog occurs at

325 speeds above 10 m s^{-1} (Filonczuk et al., 1995). Fog rarely occurs in calm conditions (Figure 4b), suggesting an optimal

326 wind speed range for its formation and warranting further exploration, as the role of wind speed on turbulence and

327 surface heat fluxes, as highlighted by Gultepe et al. (2007), significantly influences fog. While the influence of SST

328 was initially assessed by comparing SAT measurements from the airport with SST data from the oceanographic

329 station, a more comprehensive understanding is obtained by examining the effect of the sea to the west and east of the

330 airport. To achieve this, satellite-derived SST values for the regions west and east of the airport (Figure 1b) were

331 analyzed. These areas correspond to the directions of the two prevailing winds most commonly associated with fog

332 formation at Pula Airport. Scatterplots of SAT versus SST were generated for the eastern and western regions,

333 encompassing all observations, as well as those specifically under fog and mist conditions (Figure 7). A visual analysis

334 indicates that fog and mist typically form when SAT-SST pairs are associated with lower values. A more detailed

335 analysis reveals that fog data points (squares) in the western region are more dispersed, indicating greater variability

336 in SST for the same SAT, while the eastern region shows a more consistent SST-SAT relationship. Statistical analysis

337 supports this observation, with the standard deviation of SST for fog observations being 3.55 °C in the western area

338 and 3.37 °C in the eastern area. For mist, the standard deviation is 4.03 °C in the western area and 3.83 °C in the

339 eastern area. To further investigate the role of SST in fog formation in fog formation, differences in SST between the

340 western and eastern regions were analyzed under various conditions (Figure 8). When neither fog nor mist is present,

341 SST in the western area is slightly higher than in the eastern area. During fog events, however, the pattern reverses,

342 with SST being higher in the eastern area. In contrast, mist typically occurs when SST is higher in the western area

343 than in the eastern area. These differences align with the prevailing wind directions observed during fog and mist

344 events (Figure 4). During fog, winds that are predominantly from the west to northwest (W-NW) promote cooling in

345 the western area. Winds from the east (E) during mist contribute to reduced SST in the eastern region. Despite these

346 variations, the SST differences between the two areas are small, rarely exceeding 0.5 °C.

347
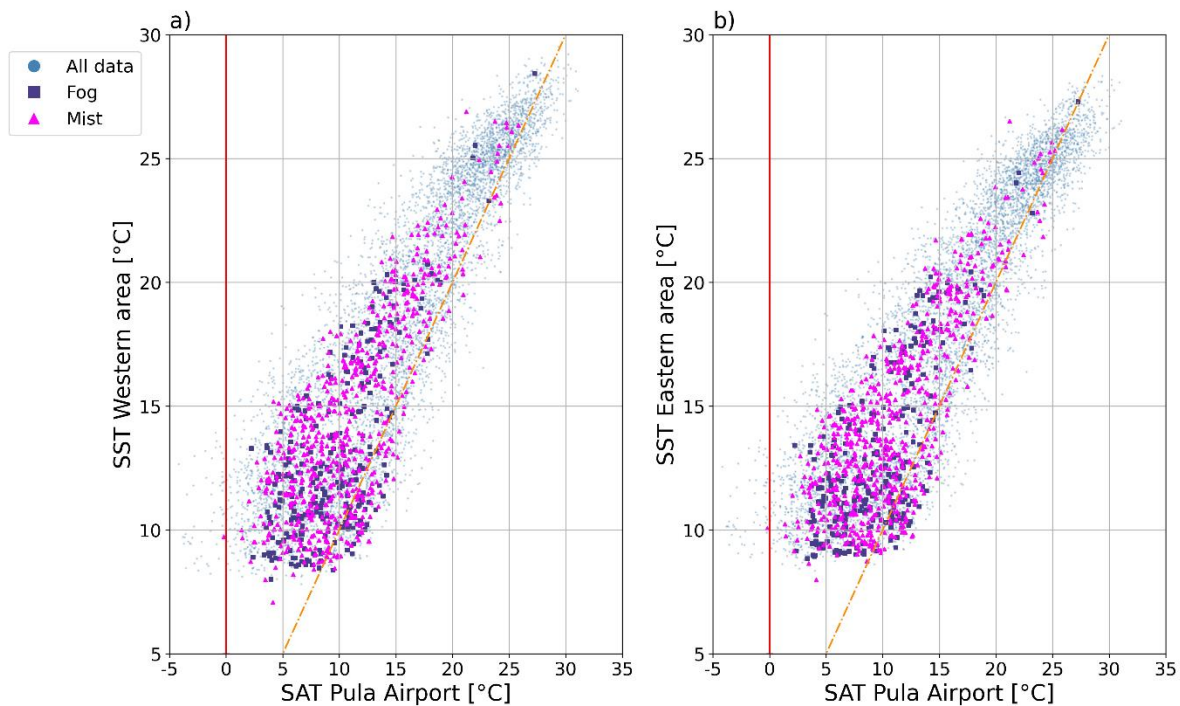
349 **Figure 7. Scatter plots of satellite sea surface temperature (SST) for western area (a) and eastern area (b), and surface air**
350 **temperature (SAT) at Pula Airport, 2001.-2020. The vertical red line indicates SAT=0 °C, and the dotted diagonal orange**
351 **line indicates SAT=SST.**

352
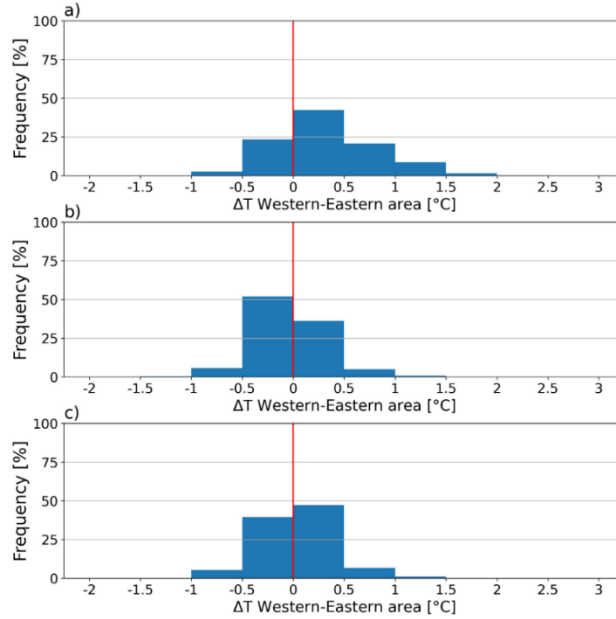
Figure 8. Histograms of satellite SST difference between the western and eastern area for observations without fog and mist (a), fog (b) and mist(c).

3.2 GNG analysis of synoptic weather patterns

In this analysis, the GNG method was applied to identify characteristic temporal and spatial patterns in wind and MSLP fields associated with the formation of fog and mist in the Pula region. The analysis was conducted on a monthly basis, processing data for each month (e.g., all January data, all February data) separately. This approach was chosen to improve the interpretability of the results, to take seasonality into account and to reduce the computational effort, especially given the large size of the hourly dataset. To save resources, the GNG algorithm was applied exclusively to 10 m wind data from ERA5, with the derived pressure fields being extrapolated afterwards. The derived pressure field corresponds to the mean pressure field associated with each BMU. Once the BMUs were identified, all pressure fields corresponding to the time instances of each BMU were retrieved and averaged to calculate the mean pressure field for each BMU. To obtain an appropriate synoptic situation with large wind systems, such as anticyclones and cyclones affecting the northern Adriatic, a large area in the Mediterranean was selected for analysis (Figure 1b). The analysis utilized 40 years of ERA5 data (1979–2019), providing extensive time series data to enable the GNG algorithm to derive robust and accurate spatio-temporal patterns. Notably, there is a one-year discrepancy between the ERA5 dataset and the fog dataset (2020) due to the GNG analysis being completed before this study began, and the computational resources required for a new analysis were unavailable. Since the wind was the primary variable and the MSLP was derived by averaging numerous synoptic situations, the wind had the dominant influence. This approach excluded the occurrence of extreme cyclonic systems (MSLP < 1000 hPa) or anticyclonic (MSLP > 1030 hPa) from the results. For example, deep cyclones, which are extremes, are smoothed, and while BMUs can indicate their locations, the exact pressure values are not retained. However, from a conceptual point of view, the interaction between high and low pressure systems and the location of these systems and their associated winds match well with the climatology of the region.

376 This process generated 9 Best Matching Units (BMUs) for each month (a total of 108 BMUs) distributed across hourly
377 data, representing the weather patterns with the highest variance. Hourly data were then aggregated into daily data by
378 identifying the most frequently occuring BMU within a day. For the 2001–2019 period, each day with fog or mist was
379 assigned to its corresponding dominant BMU, providing a synoptic weather pattern classification for fog and mist
380 days at Pula Airport. To focus on the prevailing synoptic patterns that contribute to the formation of fog and mist, the
381 months from October to March (Figure 2b) were examined in more detail (Table 1). In this way, 85 % of the variability
382 could be captured. Then, for each month, the first BMUs whose sum of their contributions to the variability exceeded
383 the threshold of 60 % were selected. In this way, a total of 18 BMUs were included in the further analysis, which is
384 significantly fewer than 54 BMUs (6 months multiplied by 9 BMUs). By selecting 2 to 4 BMUs for each month based
385 on the criteria described above, the study captured more than 60 percent of the events for each analyzed month.
386
387 **Table 1. Display of the most frequent Best Matching Units (BMUs) (the first BMUs for each month whose sum of their**
388 **contributions to the variability exceeded the threshold of 60 %) describing the prevailing synoptic weather pattern during**
389 **the days with fog and mist for the selected month at Pula Airport, 2001-2019. The slope coefficients describe the linear**
390 **trends of the most common BMUs, i.e. the yearly change in frequency, and they are also used to generate the graphs of the**
391 **linear trends in Figure 14.**

Month	BMU	Synoptic pattern	Wind	Slope coeff.	Frequency (fog)		Frequency (mist)	
					#	%	#	%
January	BMU-1-6	Quasi-non-gradient-field	WNW, W	-0.390	30	54 %	68	39 %
	BMU-1-8	Cyclone over northern Adriatic (MSLP<1008 hPa)	NW	0.107	11	20 %	39	23 %
February	BMU-2-5	Anticyclone over central/western Europe (MSLP>1028 hPa)	NE, NNE	0.006	8	16 %	13	12 %
	BMU-2-6	Quasi-non-gradient-field	SSW	-0.138	17	33 %	36	32 %
	BMU-2-7	Cyclone over northern Adriatic (MSLP<1008 hPa)	NW	-0.025	7	14 %	59	38 %
March	BMU-3-1	Anticyclone over southeastern Europe (MSLP>1022 hPa)	SSE	-0.572	16	16 %	5	16 %
	BMU-3-3	Cyclone over northern Adriatic (MSLP<1006 hPa)	SE	-0.051	6	19 %	25	25 %
	BMU-3-8	Quasi-non-gradient-field	SSE	0.255	11	35 %	31	39 %
October	BMU-10-1	Anticyclone over southeastern Europe (MSLP>1018 hPa)	NE	0.158	4	16 %	13	11 %
	BMU-10-5	Anticyclone over southeastern Europe (MSLP>1020 hPa)	SE	-0.272	10	40 %	38	32 %
	BMU-10-6	Quasi-non-gradient-field	SE	-0.051	4	16 %	27	23 %
November	BMU-11-5	Anticyclone over eastern Europe (MSLP>1024 hPa)	SE	0.251	8	24 %	23	21 %
	BMU-11-7	Quasi-non-gradient-field (MSLP>1022 hPa)	WSW	-0.415	6	18 %	29	26 %
	BMU-11-9	Anticyclone over southeastern Europe (MSLP>1026hPa)	ENE	-0.041	11	33 %	28	25 %
December	BMU-12-1	Anticyclone over southeastern Europe (MSLP>1026 hPa)	S	-0.000	7	21 %	31	21 %
	BMU-12-3	Cyclone over southern Adriatic (MSLP<1008 hPa)	NE	0.266	5	15 %	23	15 %
	BMU-12-4	Cyclone over the Tyrhennian Sea (MSLP<1008 hPa)	NE	-0.470	6	18 %	14	9 %
	BMU-12-8	Anticyclone over central and eastern Europe (MSLP >1030 hPa)	NE	-0.130	3	9 %	23	15 %

392

393   The analysis of synoptic patterns associated with fog formation (Table 1) indicates that in January, the dominant
394   conditions favoring fog and mist in Pula are characterized by a quasi-non-gradient field across the region (BMU-1-6,
395   Figure 9a), with a very weak mean pressure gradient (Belušić Vozila et al., 2021). This stable atmospheric pattern
396   supports the persistence of calm and stagnant air masses over Pula, limiting the dispersion of moisture and pollutants
397   and thereby enabling fog formation. The second most common synoptic pattern conducive to the formation of fog and
398   mist features a cyclone over the northern Adriatic (BMU-1-8, Figure 9c). Both synoptic patterns support weak
399   WNW/NW winds over the Istrian peninsula (Figure 9b and 9d). A similar synoptic pattern persists during the transition
400   into February and March. The cyclone over the northern Adriatic is the most frequent pattern suitable for the formation
401   of mist in February (BMU-2-7, Figure 10a) and the second most frequent in March (BMU-3-3, Figure 10e). The
402   difference is the prevailing NW wind in February (Figure 10b), while March is characterized by SE winds (Figure
403   10f). The quasi-non-gradient pressure field is the most common pattern favorable for both fog and mist formation in
404   March (BMU-3-8, Figure 10g), and the second most common for fog and the most common for mist in February
405   (BMU-2-6, Figure 9g). SSW winds are observed in February (Figure 9h), whereas March is associated with weaker
406   SSE winds (Figure 10d). In addition to the quasi-non-gradient field, favorable synoptic patterns in both February and
407   March also include anticyclones over continental Europe (BMU-2-5, Figure 9e and BMU-3-1, Figure 10c).

409   Fog events are rare in Pula from April to September, and as a result, the BMU analysis does not reveal clear patterns.
410   The infrequent occurrence of fog during this period is attributed to lower relative humidity and the more stable
411   atmospheric conditions typical of summer in the region. However, local factors, such as the sea/land breeze, may
412   influence fog formation. Therefore, any analysis based on data from these months should be interpreted with caution,
413   as the number of recorded fog events is limited.

415   At the beginning of October, synoptic conditions favorable for the occurrence of fog and mist in Pula are typically
416   characterized by high pressure over continental Europe, with the most common pattern being the center of the high-
417   pressure system positioned over southeastern Europe, which supports SE winds (BMU-10-5, Figure 11c and 11d).
418   This anticyclonic pattern persists into November, accompanied by a strengthened pressure field and intensified
419   pressure gradients over the central Mediterranean, conditions which promote fog development in the region (BMU-
420   11-9, Figure 12e and 12f). The intensified synoptic pressure gradients over the central Mediterranean contribute to
421   increased NE wind patterns. This increased wind activity can result in moist air being transported from the sea to the
422   coastal regions, providing an additional source of moisture for fog formation. The convergence of air masses along
423   these enhanced pressure gradients likely induces upward motion of air, which can result in adiabatic cooling and an
424   increase in relative humidity, creating conditions favorable to fog and mist formation. Pula's coastal location amplifies
425   the influence of the anticyclone. Coastal areas are more prone to temperature inversions due to the sea's heat retention,
426   which reduces temperature fluctuations. Anticyclonic conditions over Eastern Europe combined with coastal
427   geography create an environment where cool, moist air is trapped near the surface, favoring the formation of fog. The
428   conditions that favor mist formation are varied; the most common synoptic pattern is the one where the high-pressure
429   area is located over the western Mediterranean and WSW winds over the Istrian peninsula. In addition to the

430 anticyclone, a quasi-non-gradient field is also present in October and November (BMU-10-6, Figure 11e, 11f and

431 BMU-11-7, Figure 12c and 12d). In December, the prevailing synoptic weather patterns associated with fog and mist

432 become harder to identify, with BMUs more evenly distributed and more dynamic conditions, similar to those in

433 February and March. Nonetheless, the most frequent synoptic pattern for fog and mist (BMU-12-1, Figure 13a and

434 BMU-12-8, Figure 13g) has anticyclonic characteristics. Under these conditions, the Pula region is under the influence

435 of a pressure ridge, with the prevailing weak wind patterns from the S and NE further increasing the probability of

436 fog formation (Figure 13b and 13h). Compared to earlier months, cyclones also play a more pronounced role in

437 December's fog and mist formation. This influence is observed in two ways: weak NE winds associated with cyclonic

438 conditions in the southern Adriatic (BMU-12-3, Figure 13c, 13d) and stronger NE winds due to cyclonic conditions

439 in the Tyrrhenian Sea (BMU-12-4, Figure 13e, 13f).

440

441 In summary, most fog and mist events during the cold season occur under stable anticyclonic or quasi-non-gradient

442 conditions (13 total), though some events also occur under low-pressure conditions (5 total). WNW/W winds are most

443 common in January and February under quasi-non-gradient fields and they contribute significantly to fog formation.

444 SE winds dominate in March and October under anticyclonic conditions. Northeasterly winds are predominant in

445 December, often in conjunction with anticyclones. The quasi-non-gradient field is the most-frequent weather situation,

446 accounting for 40% of fog cases and 37% of mist cases, followed by anticyclones, which account for 39% of fog cases

447 and 33% of mist cases. Cyclones are less common, accounting for 21% of fog cases and 30% of mist cases.
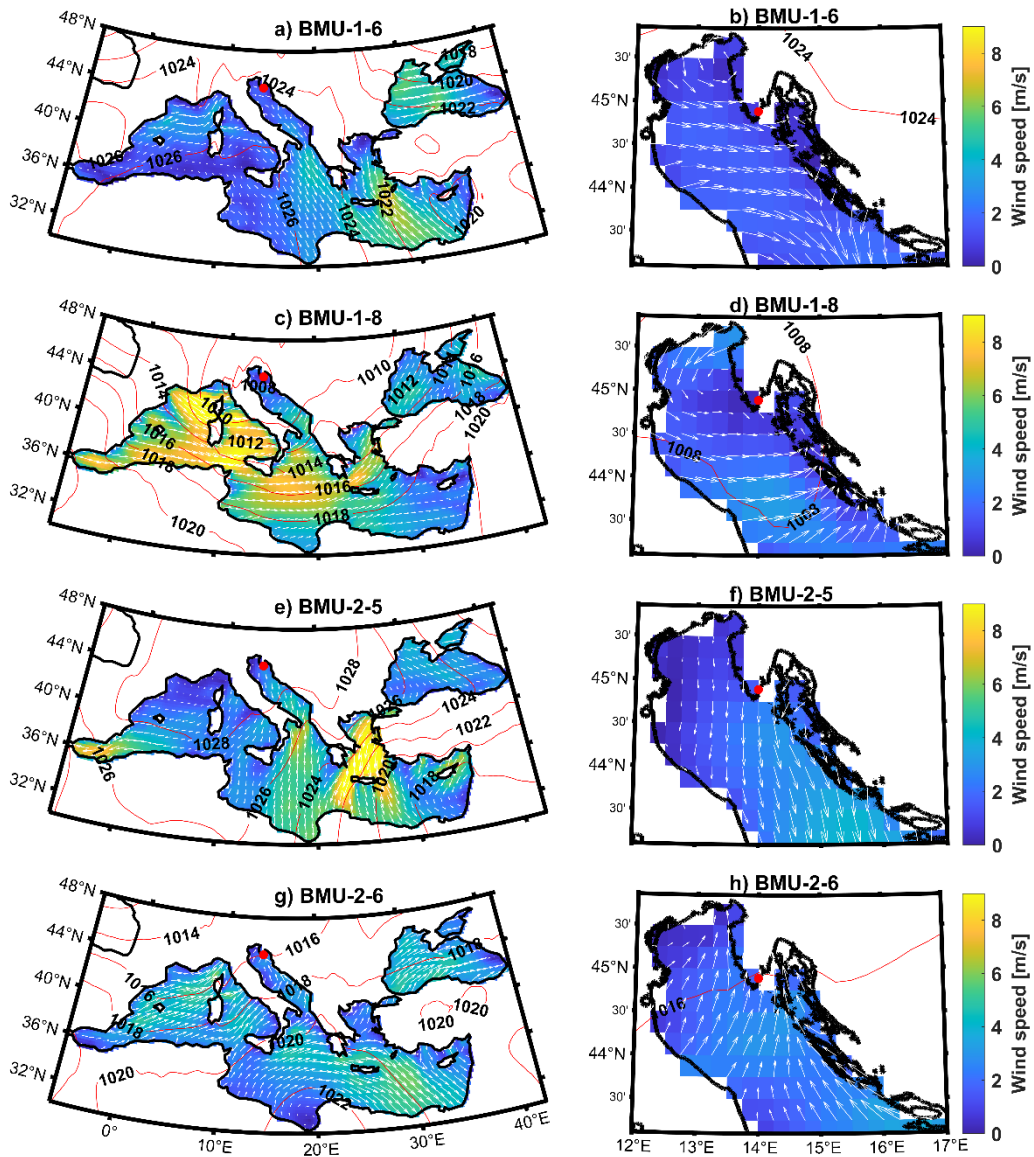
Figure 9. Prevailing Best Matching Units (BMUs) describing the synoptic patterns favoring the formation of fog and mist at Pula Airport in January (a, c) and February (e, g) for the wider Mediterranean region. The red dot marks the location of Pula Airport. The red contour lines show the mean sea level pressure (MSLP). The contours represent the amplitude of the wind speed, above which the wind vectors are represented by arrows (every third vector has been drawn). The same principle applies to the zoomed area of the northern and central Adriatic for January (b, d) and February (f, h), but here each vector is plotted.

456
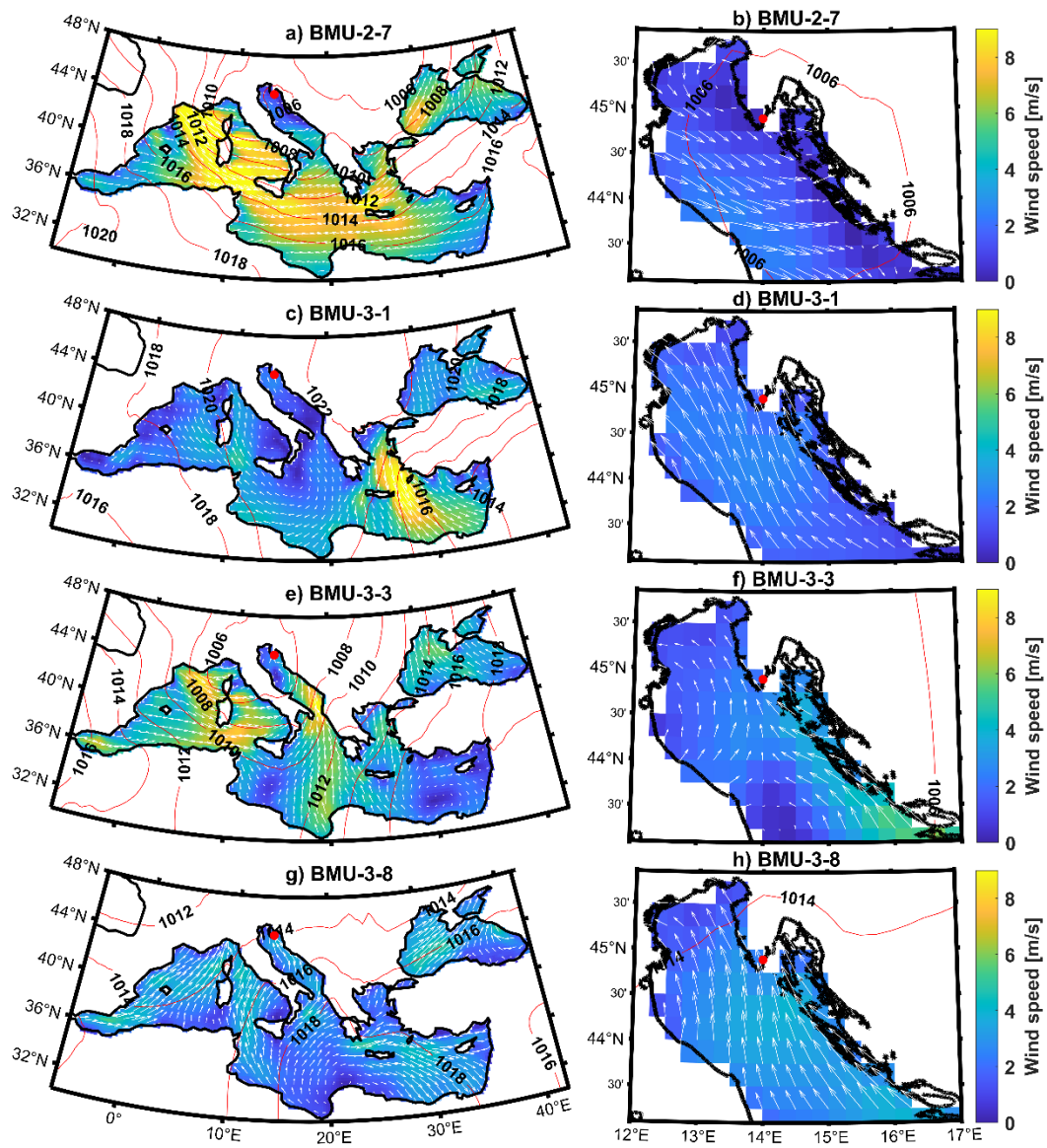
457 **Figure 10. Similar to Figure 9, but for February (a) and March (c, e, g) in the wider Mediterranean area, and for the**
458 **northern and central Adriatic: February (b) and March (d, f, h) in the zoomed-in area.**

459
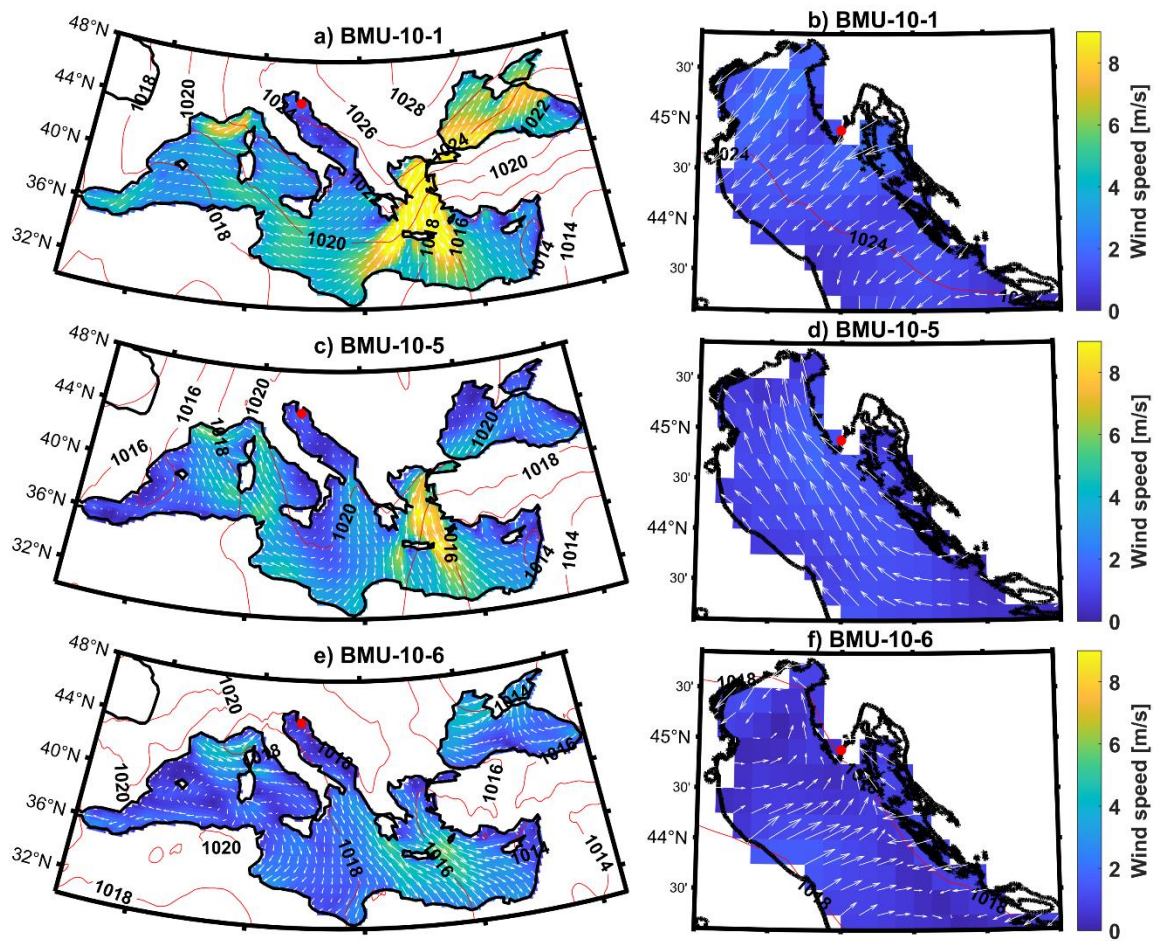
460
Figure 11. Similar to Figure 9, but for October: (a, c, e) show the wider Mediterranean area, while (b, d, f) focus on the northern and central Adriatic.
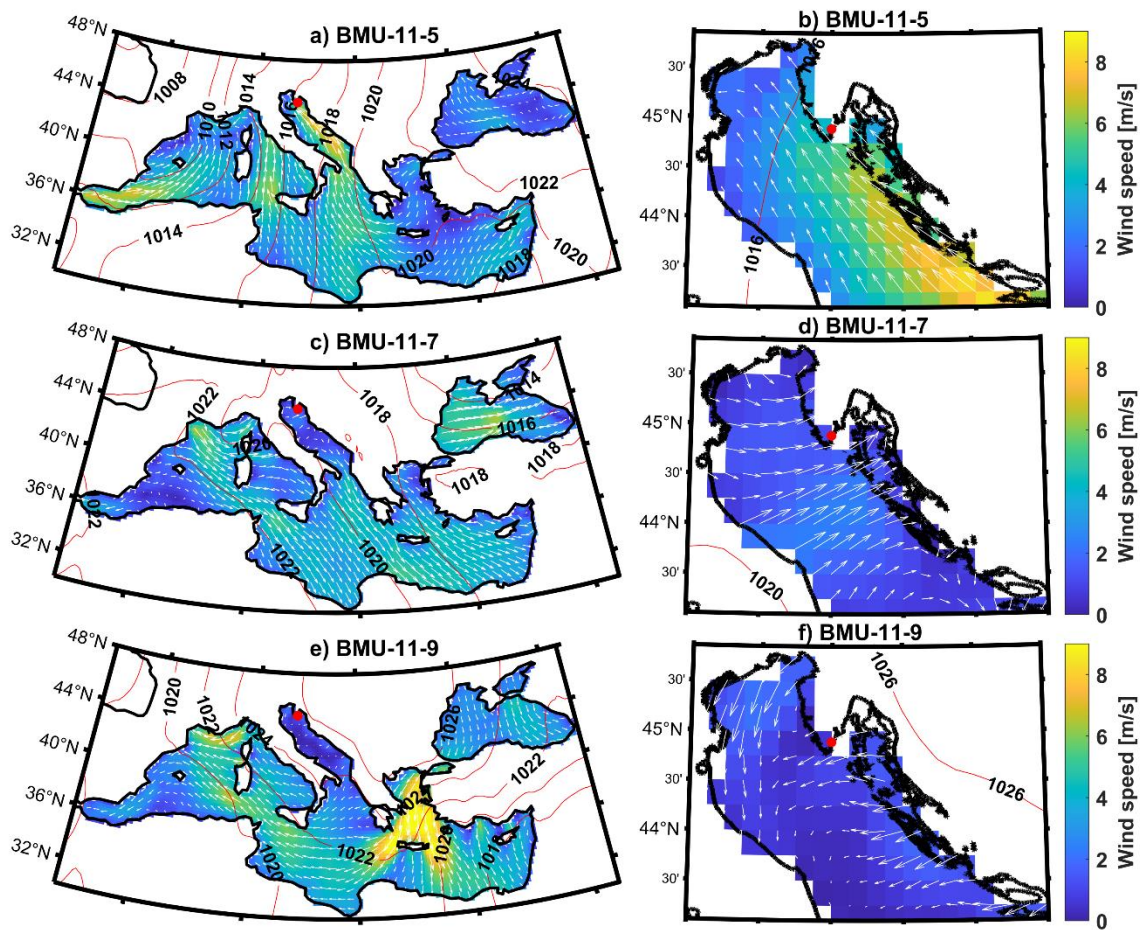
463
464 **Figure 12. Similar to Figure 9, but for November: (a, c, e) show the wider Mediterranean area, while (b, d, f) focus on the**
465 **northern and central Adriatic.**
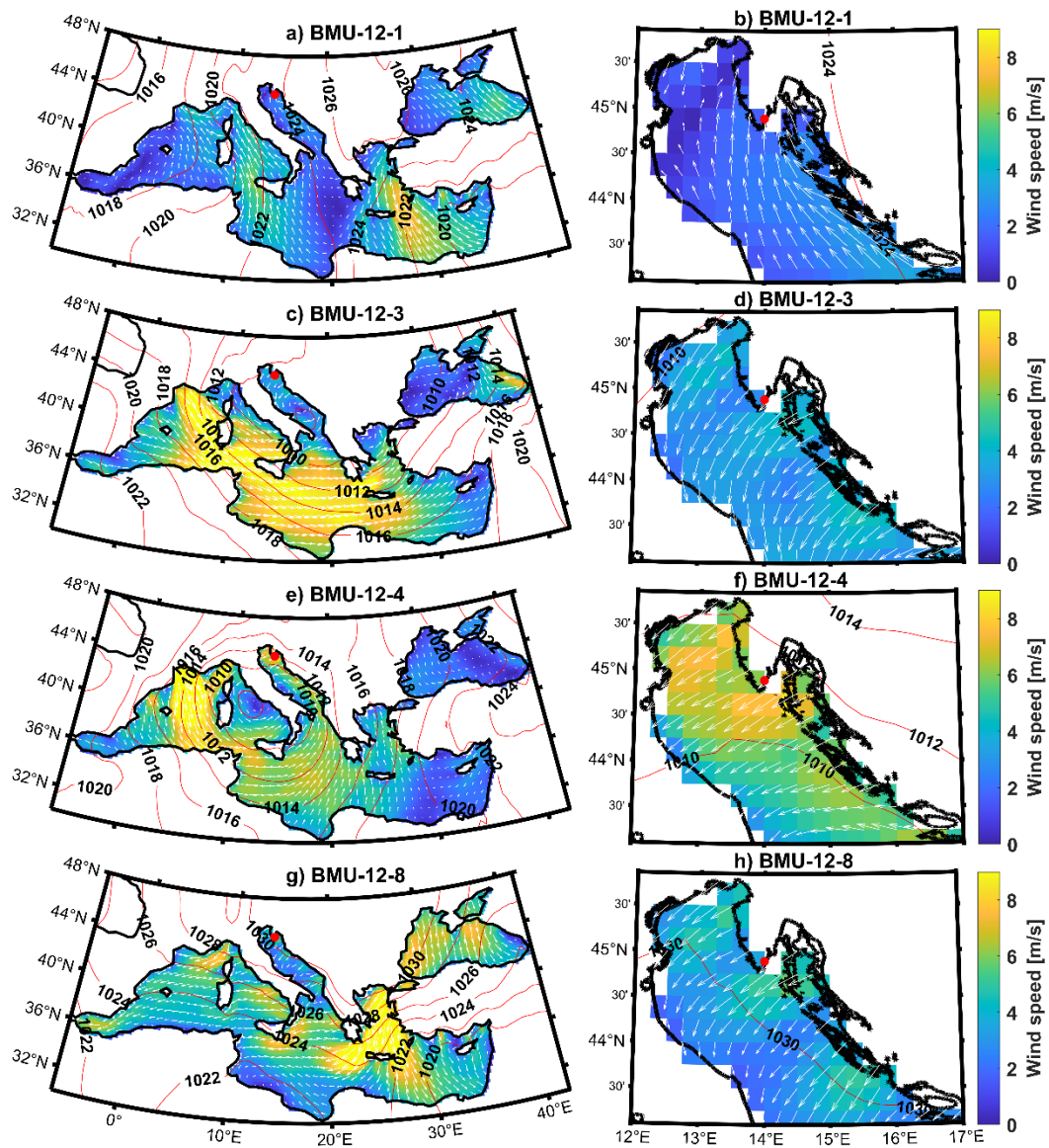
466
467 **Figure 13. Similar to Figure 9 but for December: (a, c, e, g) show the wider Mediterranean, while (b, d, f, g) focus on the**
468 **northern and central Adriatic.**
469
470
471
472
473
474
475
476
477
478
479
480
481

In addition to examining the prevailing synoptic patterns during the occurrence of fog and mist, the GNG analysis also allows for the investigation of the time series of frequencies of individual BMUs. This was accomplished by first calculating the relative monthly frequency of each BMU for each year, followed by using linear regression to estimate trends and calculate slope coefficients. This process provides insights into changes in the frequency of each BMU over two decades (Table 1, Figure 14). In January, the more frequent BMU-1-6 (Figure 14a) has a strong negative trend of -0.390, while the less frequent BMU-1-8 (Figure 14b) has a weaker positive trend of 0.107. In February, the most frequent BMU-2-7 (Figure 14e) has a weak negative trend of -0.025. In March, the most frequent BMU, BMU-3-8 (Figure 14h) has a positive trend of 0.255, while BMU-3-1 (Figure 14f) has a strong negative trend of -0.572. In October, the most frequent BMU for fog and mist (BMU-10-5, Figure 14j) has a negative trend (-0.272), while in November and December there is almost no trend for the most frequent BMUs (BMU-11-9, Figure 14n and BMU-12-1, Figure 14o). It can be summarized from the table that the BMUs most associated with the occurrence of fog and mist exhibit negative trends in the months with the highest share, January and February. Analyzing the data by counting positive and negative changes and grouping the synoptic patterns into three categories (cyclonic/anticyclonic/quasi-non-gradient field) reveals that out of the 18 BMUs, 8 are anticyclonic, 5 are quasi-non-gradient, and 5 are cyclonic. There is no trend for BMU-12-1 in the anticyclonic group; 3 BMUs increase in frequency and 4 BMUs decrease in frequency. In the quasi-non-gradient group, there is 1 increase and 4 decreases. This decline in quasi-non-gradient synoptic situations has already been documented during the summer months (Belušić Vozila et al., 2021). Of the 5 cyclonic BMUs, 2 increase in frequency and 3 decrease. Additionally, a significant decrease (slope coefficient >0.3 or <-0.3) is observed in BMU-3-1 (anticyclonic), BMU-1-6 (quasi-non-gradient field), and BMU-12-4 (cyclonic). Positive trends do not show such large slope coefficients.
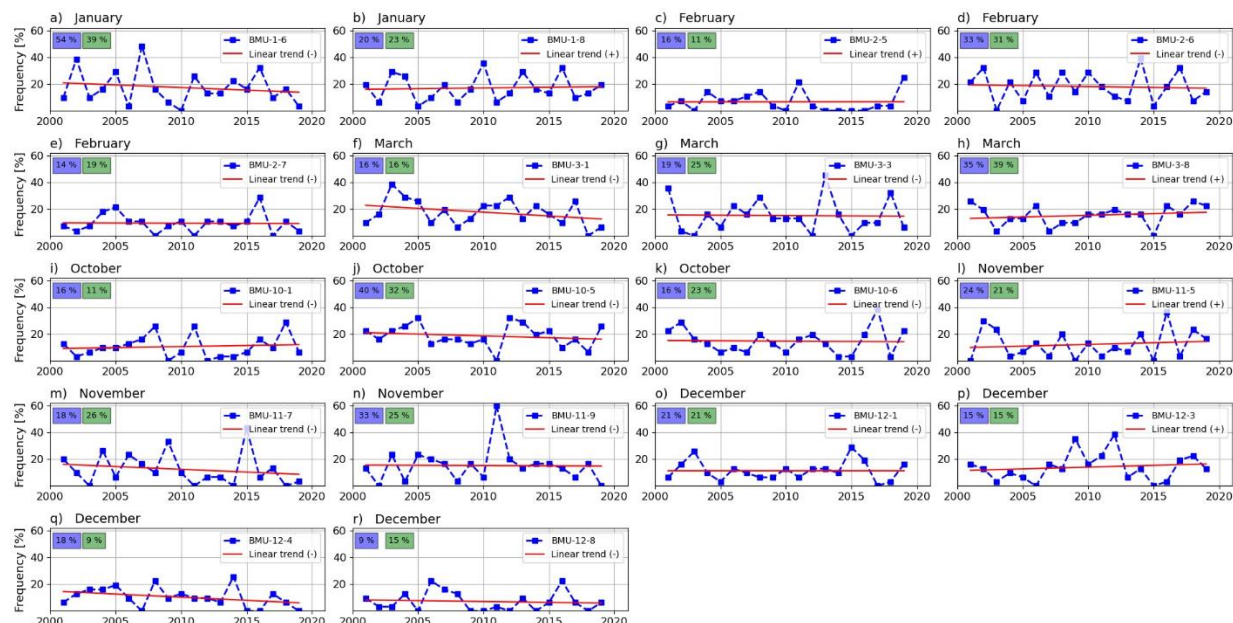
Figure 14. Relative frequencies and trends of most common (monthly share in days with fog/mist greater than 15%) BMUs for fog and mist in Pula Airport, data period: 2001-2019. Numbers shaded in blue denote the share of a BMU for fog days, numbers shaded in green denote the share of a BMU for mist days. The slope coefficient values for the linear trends can be found in Table 1.

4 Conclusion

This comprehensive climatological analysis of fog and mist occurrences at Pula Airport from 2001 to 2020 has provided valuable insights into the changing patterns of these meteorological phenomena. By combining classical statistics and neural networks, the study produced noteworthy results.

The frequency of occurrence of fog and mist at Pula airport has been decreasing, similar to trends observed in other European locations. While reduced air pollution explains the decline in cities like Zagreb and Milan, this is less applicable to Pula due to its smaller size and lower industrial impact. Climate change, including both rising air temperatures as well as increased sea surface temperatures, is a key driver of this trend. Additionally, changing wind patterns also influence fog formation by affecting temperature gradients and evaporation rates.

Fog at Pula airport occurs mainly during the cold season (October-March) and is primarily associated with weak westerly and northwesterly winds. It is more likely to occur when the sea surface temperature is higher than the air temperature. Mist has similar characteristics to fog, although it is more likely to occur with easterly winds. Wind direction and SST variations between the sea to the west and east of the airport influence fog and mist formation.

Most fog and mist events during the cold season occur under stable anticyclonic or quasi-non-gradient conditions, with the latter being the most frequent. Wind patterns vary seasonally, with WNW/W winds in January and February aiding fog formation, SE winds prevailing in March and October, and northeasterly winds dominating in December under anticyclones.

Synoptic patterns that promote fog and mist, especially quasi-non-gradient situations, are declining. This reduction weakens winds that transport moisture from the sea to the land, influenced by rising sea surface and air temperatures. As a result, fog and mist frequency is expected to continue decreasing.

Overall, these findings provide a strong foundation for further research, facilitating a deeper understanding of the meteorological and oceanographic factors that influence fog and mist at Pula Airport. This is especially significant as it marks the first scientific study on fog in the Pula region in over 50 years, a period during which climate change has notably impacted the local climate. This study has taken on the broad task of identifying synoptic patterns conducive to fog and mist formation. Since fog and mist are mainly influenced by wind speed and moisture advection, there is potential for coupled atmospheric-oceanographic modeling that incorporates local topography and enhances the parameterization of processes at finer temporal and spatial scales. Such advancements would provide a more comprehensive understanding of local meteorological phenomena and their implications for various applications, including aviation meteorology and environmental monitoring.

Code/data availability

All data and codes used in the analysis are available from the corresponding author on request.

Author contribution

Marko Zoldoš and Tomislav Džoić equally contributed to the conception and design of the study, material collection, data preparation, statistical and neural network analysis, creation of the figures and writing. Frano Matić contributed to the neural network analysis. All authors have read and approved the final manuscript.

Competing interests

The authors declare that they have no conflict of interest.

Acknowledgments

Frano Matić was supported in part by the European University of the Seas (SEA-EU) alliance through collaborative efforts and resources. Measurements and observations for Pula Airport were provided by the Croatian Air Navigation Service (Crocontrol Ltd.). SST data for Pula were provided by the Meteorological and Hydrological Service of Croatia (DHMZ). SST data in the Mediterranean region were downloaded from the Copernicus Marine Data Store (https://data.marine.copernicus.eu/). 10-m wind and mean sea-level pressure (MSLP) data were adopted from the fifth generation of ECMWF's ERA5 reanalysis of global climate and weather. Final proofreading (grammar/spelling check) was performed by ChatGPT from OpenAI.

References

Allan, S.S., Gaddy, S.G., Evans, J.E.: Delay causality and reduction at the New York City airports using terminal weather information systems, Massachusetts Institute of Technology, Lincoln Laboratory, Project Rep. ATC-291, 2001

Belo-Pereira, M., Santos, J.A.: A persistent wintertime fog episode at Lisbon airport (Portugal): performance of ECMWF and AROME models, Meteorol. Appl. 23, 353-370, doi:10.1002/met.1560, 2016

Bendix, J.: Fog climatology of the Po Valley, Riv. Meteorol. Aeronau. 54(3-4), 25-36, 1994

Belušić, A., Prtenjak, M.T., Güttler, I., Ban, N., Leutwyler, D., Schär, C.: Near-surface wind variability over the broader Adriatic region: insights from an ensemble of regional climate models, Clim. Dyn. 50, 4455–4480, doi:10.1007/s00382-017-3885-5, 2018

Belušić Vozila, A., Telišman Prtenjak, M., Güttler, I.: A weather-type classification and its application to near-surface wind climate change projections over the Adriatic region, Atmosphere 12, 948, doi:/10.3390/atmos12080948, 2021

Bergot, T., Koračin, D.: Observation, simulation and predictability of fog: review and perspectives, Atmosphere 12(2), 235, doi:10.3390/atmos12020235, 2021

574 Bonacci, O. (2010): Analysis of mean annual temperature series in Croatia, Građevinar, 62(9), 781-791,

575 https://hrcak.srce.hr/59611, 2010

576 Bonacci, O.: Relationship between sea surface temperature (SST) and surface air temperature (SAT) along the eastern

577 Adriatic coast of Croatia, Vodoprivreda, 55, 325/326; 167-183, 2023

578 Duynkerke, P.G.: Radiation fog: A comparison of model simulation with detailed observations, Mon. Weather Rev.

579 119(2), 324-341, doi:10.1175/1520-0493(1991)119<0324:RFACOM>2.0.CO;2, 1991

580 Džoić, T., Zorica, B., Matić, F., Šestanović, M., Čikeš Keč, V.: Cataloguing environmental influences on the

581 spatiotemporal variability of Adriatic anchovy early life stages in the eastern Adriatic Sea using an artificial neural

582 network, Front. Mar. Sci. 9, 997937, doi:10.3389/fmars.2022.997937, 2022

583 Filonczuk, M.K., Cayan, D.R., Riddle, L.G.: Variability of marine fog along the California coast, Scripps Institution

584 of Oceanography Report 95-2, 102 pp., 1995

585 Fritzke, B.: A growing neural gas network learns topologies, Adv. Neural Inf. Process. Syst. 7, 625–632, 1995

586 Gultepe, I., Milbrandt, J.A.: Microphysical observations and mesoscale model simulation of a warm fog case during

587 FRAM project, Pure Appl. Geophys 164, 1161-1178, doi:10.1007/978-3-7643-8419-7_4, 2007

588 Gultepe. I., Tardif, R., Michaelides, S.C., Cermak, I., Bott, A., Bendix, J., Müller, M.D., Pagowski, M., Hansen, B.,

589 Ellrod, G., Jacobs, W., Toth, S., Cober, S.G.: Fog research: a review of past achievements and future perspectives,

590 Pure and Appl. Geophys. 164(6-7), 1121-1159, doi:10.1007/s00024-007-0211-x, 2007

591 Hersbach, H.; Bell, B.; Berrisford, P.; Hirahara, S.; Horányi, A.; Muñoz-Sabater, J.; Nicolas, J.; Peubey, C.; Radu, R.;

592 Schepers, D.; Simmons, A.; Soci, C.; Abdalla, S.; Abellan, X.; Balsamo, G.; Bechtold, P.; Biavati, G.; Bidlot, J.;

593 Bonavita, M.; De Chiara, G.; Dahlgren, P.; Dee, D.; Diamantakis, M.; Dragani, R.; Flemming, J.; Forbes, R.; Fuentes,

594 M.; Geer, A.; Haimberger, L.; Healy, S.; Hogan, R. J.; Hólm, E.; Janisková, M.; Keeley, S.; Laloyaux, P.; Lopez, P.;

595 Lupu, C.; Radnoti, G.; de Rosnay, P.; Rozum, I.; Vamborg, F.; Villaume, S.; Thépaut, J.-N. (2020a): The ERA5 global

596 reanalysis, Q. J. R. Meteorol. Soc. 146, 1999–2049, doi:10.1002/qj.3803, 2020

597 Hersbach, H.; Bell, B.; Berrisford, P.; Hirahara, S.; Horányi, A.; Muñoz-Sabater, J.; Nicolas, J.; Peubey, C.; Radu, R.;

598 Schepers, D.; Simmons, A.; Soci, C.; Abdalla, S.; Abellan, X.; Balsamo, G.; Bechtold, P.; Biavati, G.; Bidlot, J.;

599 Bonavita, M.; De Chiara, G.; Dahlgren, P.; Dee, D.; Diamantakis, M.; Dragani, R.; Flemming, J.; Forbes, R.; Fuentes,

600 M.; Geer, A.; Haimberger, L.; Healy, S.; Hogan, R. J.; Hólm, E.; Janisková, M.; Keeley, S.; Laloyaux, P.; Lopez, P.;

601 Lupu, C.; Radnoti, G.; de Rosnay, P.; Rozum, I.; Vamborg, F.; Villaume, S.; Thépaut, J.-N. (2020b): ERA5 hourly

602 data on pressure levels from 1979 to present, Copernicus Climate Change Service (C3S) Climate Data Store (CDS),

603 doi:10.1002/qj.3803, 2020

604 Huang, B., Zhang, J., Cao, Y., Gao, X., Ma, S., Sun, C.: Improvements of sea fog forecasting based on CMA-TYM,

605 Front. Earth Sci. 10: 854438, doi: 10.1016/j.jastp.2022.105958, 2022

606 Ju, T., Wu, B., Zhang, H., Liu, J.: Parameterization of radiation fog-top height and methods evaluation in Tianjin,

607 Atmosphere 11(5), 480, doi:10.3390/atmos11050480, 2020

608 Kawai, H., Koshiro, T., Endo, H., Arakawa, O., Hagihara, Y., Changes in marine fog in a warmer climate., Atmos.

609 Sci. Lett. 17, 548-555, doi:10.1002/asl.691

Klaić Z. B., Pasarić Z., Tudor M.: On the interplay between sea-land breezes and etesian winds over the Adriatic, J. Mar. Sys. 78, 101–118, doi: 10.1016/j.jmarsys.2009.01.016, 2009

Klemm, O., Lin, N.: What causes observed fog trends: air quality or climate change? Aerosol. Air. Qual. Res. 16, 1131-1142, doi:10.4209/aaqr.2015.05.0353

Koračin, D., and Dorman, C.E. (Eds): Marine fog: challenges and advancements in observations and forecasting, Springer Atmospheric Sciences Series, Springer International Publishing, Cham, Switzerland, 537 pp., doi:10.1007/978-3-319-45229-6_7, ISBN 978-3-319-45227-2, 2017

Koračin, D., Lewis, J., Thompson, W.T., Dorman, C.E., Businger, J.A.: Transition of stratus into fog along the California coast: observations and modeling, J. Atmos. Sci. 58, 1714-1731, doi:10.1175/1520-0469(2001)058%3C1714:TOSIFA%3E2.0.CO;2, 2001

Kulkarni, R., Jenamani, R.K., Pithani, P., Konwar, M., Nigam, N., Ghude, S.D.: Loss to aviation economy due to winter fog in New Delhi during the winter of 2011-2016, Atmosphere, 10(4), 198, doi:10.3390/atmos10040198, 2019

Li, G., Cheng, L., Zhu, J., Trenberth, K.: Increasing ocean stratification over the past half-century, Nat. Clim. Change 10(12), 1-8, doi:10.1038/s41558-020-00918-2, 2020

Mariani, L.: Fog in the Po valley: Some meteo-climatic aspects, Ital. J. Agrometeorol. 3: 35-44, 2009

Martinetz, T., Schulten, K.: A "neural-gas" network learns topologies, in: Proceedings of the International Conference on Artificial Neural Networks 1991, 397-402, 1991

Matić, F., Džoić, T., Kalinić, H., Ćatipović, L., Udovičić, D., Juretić, T., Rakuljić, L., Sršen, D., Tičina, V.: Observation of abrupt changes in the sea surface layer of the Adriatic Sea, J. Mar. Sci. Eng. 10, 848, doi:10.3390/jmse10070848, 2022

Merchant, C. J.; Embury, O.; Bulgin, C. E.; Block, T.; Corlett, G. K.; Fiedler, E.; Good, S. A.; Mittaz, J.; Rayner, N. A.; Berry, D.; Eastwood, S.; Taylor, M.; Tsushima, Y.; Waterfall, A.; Wilson, R.; Donlon, C.: Satellite-based time-series of sea-surface temperature since 1981 for climate applications, Sci Data 6(1) 1-18, doi: 10.1038/s41597-019-0236-x, 2019

Omazić, B., Telišman Prtenjak, M., Prša, I., Belušić Vozila, A., Vučetić, V., Karoglan, M., Karoglan Kontić, J., Prša, Ž., Anić, M., Šimon, S., Güttler, I.: Climate change impacts on viticulture in Croatia; viticultural zoning and future potential, Int. J. Climatol. 40, 5634 – 5655, doi:10.1002/joc.6541, 2020

Oztaner, Y.B., Yilmaz, A.: An examination of fog and PM10 Relationship for Ataturk and Esenboga International Airports of Turkey, in: Proceedings of the 6th Atmospheric Science Symposium - ATMOS 2013, Istanbul Technical University, 2013

Pandžić K., Likso T.: Eastern Adriatic typical wind field patterns and large-scale atmospheric conditions, Int. J. Climatol. 25, 81–98, doi:10.1002/joc.1085, 2005

Pastor, F., Valiente, J.A., Palau, J.L.: Sea surface temperature in the Mediterranean: trends and spatial patterns, Pure and Appl. Geophys. 175, 4017-4029, doi:10.1007/s00024-017-1739-z, 2018

Pawlowicz, R.: M_Map: A mapping package for MATLAB, version 1.4m, [Computer software], available online at www.eoas.ubc.ca/~rich/map.html, 2020

646 Popović, R., Kulović, M., Stanivuk, T.: Meteorological safety of entering eastern Adriatic ports, Trans. Marit. Sci.
647 2014 (1), 53-60, doi:10.7225/toms.v03.n01.006, 2014

648 Stipaničić, V.: Fog on the western coast of the Istria peninsula, Vijesti Pomorske meteorološke službe, 18, 7-10,
649 https://library.foi.hr/dbook/cas.php?B=1&item=S02101&godina=1972&broj=00001, 1972

650 Stolaki, S.N., Kazadzis, S.A., Foris, D.V., Karacostas, Th.S.: Fog characteristics at the airport of Thessaloniki, Greece,
651 Nat. Hazards Earth Syst. Sci. 9: 1541-1549, doi:10.5194/nhess-9-1541-2009, 2009

652 Šantić, D., Piwosz, K., Matić, F., Vrdoljak Tomaš, A., Arapov, J., Dean, J. L., Šolić, M., Koblížek, M., Kušpilić, G.,
653 Šestanović, S.: Artificial neural network analysis of microbial diversity in the central and southern Adriatic Sea, Sci.
654 Rep. 11, 1–15, doi:10.1038/s41598-021-90863-7, 2021

655 Šimunić, I., Likso, T., Husnjak, S., Bubalo Kovačić, M.: Analysis of climate elements in central and western Istria for
656 the purpose of determining irrigation requirements of agricultural crops, Agric. Conspec. Sci. 86(3), 225-233,
657 https://hrcak.srce.hr/file/382381, 2021

658 Tardif, R., Rasmussen, R.M.: Event-based climatology and typology of fog in the New York City region, J, App.
659 Meteorol. Climatol., 46, 1141-1168, doi:10.1175/JAM2516.1, 2007

660 Telišman Prtenjak, M., Grisogono, B.: Sea-land breeze climatological characteristics along the northern Croatian
661 Adriatic coast, Theor. Appl. Climatol. 90, 201–215, doi:10.1007/s00704-006-0286-9, 2007

662 Telišman Prtenjak, M., Viher, M., Jurković, J.: Sea-land breeze development during a summer bora event along the
663 north-eastern Adriatic coast, Q. J. Roy. Meteorol. Soc. 136, 1554–1571, doi:10.1002/qj.649, 2010

664 Tešić, M., Brozinčević, K.: Fog phenomenon on the eastern coast of the Adriatic Sea, Hidrografski godišnjak 1974,
665 91-116, 1974

666 Tojčić, I., Denamiel, C., Vilibić, I.: Kilometer-scale trends and variability of the Adriatic present climate, (1987–
667 2017), Clim. Dyn 61, 2521–2545, 10.1007/s00382-023-06700-2

668 Tojčić, I., Denamiel, C., Vilibić, I.: Kilometer-scale trends, variability, and extremes of the Adriatic far-future climate
669 (RCP 8.5, 2070-2100), Front. Mar. sci. 16, 907–926, doi:10.3389/fmars.2024.1329020, 2024

670 Vautard, R., Yiou, P., van Oldenborgh, G.: The decline of fog, mist and haze in Europe during the last 30 years, Nat.
671 Geosci. 2, 115–119, doi:10.1038/ngeo414, 2009

672 Veljović, K., Vujović, D., Lazić, L.: An analysis of fog events at Belgrade International Airport, Theor. Appl.
673 Climatol. 119 (1-2), 13-24, doi:10.1007/s00704-014-1090-6, 2015

674 WMO, International Meteorological Vocabulary, World Meteorological Organization, Geneva, Switzerland, pp. 141.,
675 1966

676 Wang, Y., Niu, S. J., Lv, J. J., Lu, C. S., Xu, X. Q., Wang, Y. Y., Ding, J., Zhang, H., Wang, T., Kang, B.: A new
677 method for distinguishing unactivated particles in cloud condensation nuclei measurements: implications for aerosol
678 indirect effect evaluation, Geophys. Res. Lett. 46, 14185–14194, doi:10.1029/2019gl085379, 2019

679 Zoldoš, M., Jurković, J.: Fog event climatology for Zagreb Airport, Croatian Met. Journal 51(51), 13-26,
680 https://hrcak.srce.hr/168218, 2016